

FINITE DIFFERENCE TIME DOMAIN ANALYSIS OF COPLANAR TRANSMISSION LINE CIRCUITS AND A POST- GAP WAVEGUIDE MOUNTING STRUCTURE

John E. Oswald[†], Peter H. Siegel[†], Sami M. Ali[‡]

[†]Jet Propulsion Laboratory
California Institute of Technology
Pasadena, CA 91109

[‡]Ministry of PTT Telecom. College of Jeddah
Jeddah 21461
Saudi Arabia

The finite difference time domain (FDTD) method is used to calculate the S-parameters for two coplanar line filters intended for use at submillimeter wavelengths. The analysis is compared with experimental measurements made on microwave models of the two filter structures. In addition, the FDTD method is used to determine the embedding impedances of a simple post-gap waveguide mounting structure with a single backshort tuning element. The analysis results are presented as a function of backshort setting and are compared both with experimental measurements and with the results of an established theoretical model [1] of such a mounting structure.

1 Introduction

Although the finite difference time domain (FDTD) method was introduced in 1966 by K. S. Yee [2], it was not until the more recent advent of faster, more powerful computing environments that this technique has found a wide range of applicability. One of the first problems Yee considered with the FDTD method was the scattering of fields caused by conducting cylinders in free space. Now the method is being applied to the analysis of many problems including, but not limited to, microstrip filters [*e.g.*, 3] and antennas [*e.g.*, 4, 5], waveguide discontinuities [*e.g.*, 6, 7], and dielectric resonators [*e.g.*, 8].

In this paper, we demonstrate the applicability of the FDTD method to several types of problems of interest in the submillimeter wave region. First, a coplanar strip

filter designed for use at 2.5 THz is considered, and FDTD analysis is compared with scale model measurements as well as with data from Hewlett Packard's commercial program, Microwave Design System (MDS). Next, the FDTD method is used to examine a coplanar waveguide filter designed for the same purpose, and the computations are compared with the MDS calculations. Finally, a simple waveguide post-gap mounting structure with a single backshort is examined. The input impedances measured on a microwave scale model are compared to the computed values for various backshort settings.

2 Coplanar Transmission Line Circuits

Coplanar strip transmission line (twin-lead fabricated on a dielectric half space) and coplanar waveguide are ideal media for feeding a wide range of planar integrated antennas. For applications where more than one frequency will be present at the antenna terminals or where resistive or reactive matching is important it may be necessary to incorporate distributed filter elements with the feed line. Unfortunately, the limited realizable impedance range associated with twin lead makes standard high-low impedance filters difficult to implement. In cases where the size of the feed line may be an issue [e.g., 9] it is helpful to have a filter design with minimal projected area. Using the FDTD analysis in conjunction with scale model measurements we have designed distributed line band-reject filters in both coplanar stripline and coplanar waveguide. Both filters exhibit extremely narrow cross section and can be used at frequencies where the realizable thickness of the deposited metallic conductors contributes significantly to the filter characteristics.

2.1 Coplanar Strip Filter

The basic coplanar strip filter is detailed in Figure 2.1 and consists of quarter-wave high and low impedance sections which are contained within the confines of the 200Ω coplanar strips fabricated on a thick fused quartz substrate. The smallest proposed dimension is the 1 μm gap of the low impedance sections which, when combined with the 3 μm gap of the 200Ω line, gives approximately 2:1 impedance change. The filter is intended to reject the signal band centered at 2.5 THz and to pass the intermediate frequencies from 8-12 GHz in a 2.5 THz mixer. The thickness of the conducting lines ($t = 1.0 \mu\text{m}$) is a significant portion of their width so as to minimize skin effect losses for the IF. The FDTD technique was used to analyze the effects of the metal line thickness, width and air-gap as well as to determine the radiative losses, the characteristic line impedance, the effective dielectric constant, the open-circuit reference plane and the transmission properties of the coplanar strip filter. The

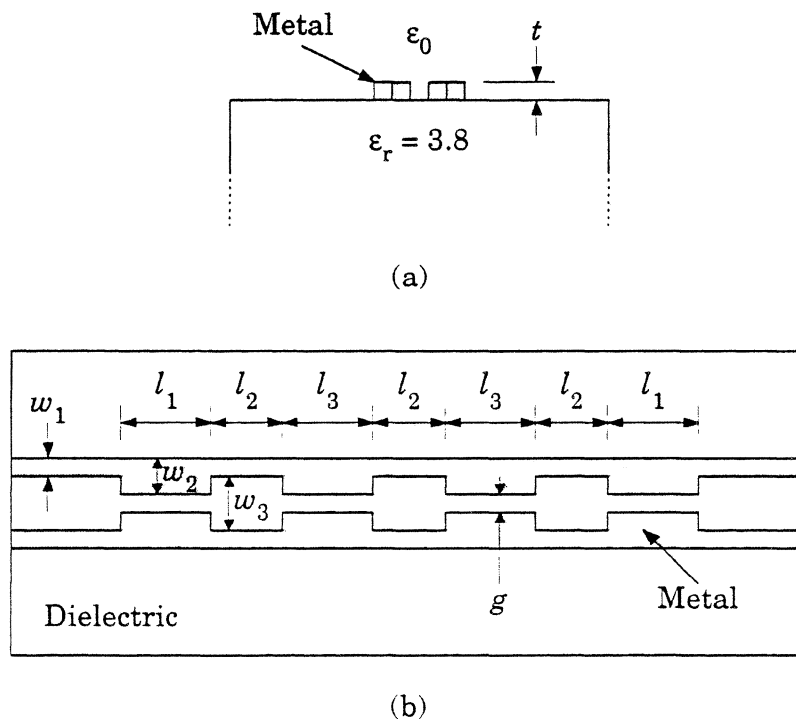


Figure 2.1 Coplanar strip filter (not to scale): (a) Cross section showing filter metal thickness on a dielectric half space; (b) Top view showing metal pattern. Dimensions (in μm) are: $t = 1.0$; $w_1 = 1.0$, $w_2 = 2.0$, $w_3 = 3.0$, $l_1 = 22.113$, $l_2 = 18.711$, $l_3 = 23.814$, $g = 1.0$.

analysis was verified using a 1680× scale model of the proposed 2.5 THz filter with a thick brass sheet to form the metallic lines and stycast $\epsilon_r = 3.8$ to model the quartz substrate. In Figure 2.2 the FDTD calculations of the S_{21} magnitude are compared with the available scale model measurements made on an HP8510 vector network analyzer. The large standing waves present in the measurements are primarily due to a mismatch between the HP8510 50Ω test cable and the ~200Ω coplanar strip line, and no correction for this has been made. Although the agreement with the measurements is not perfect, the computations accurately predict the pass band ripple pattern and the cutoff frequency as well as the radiation loss in this structure.

The filter structure of Figure 2.1 is also analyzed with the FDTD method for the case where the thickness of the metallization is $t = 0.5 \mu\text{m}$. In Figure 2.3 the S_{21} magnitude responses for filters with metal thicknesses of 0.5 and 1.0 μm are compared. Although the effect of the metal is not enormous, the figure clearly shows

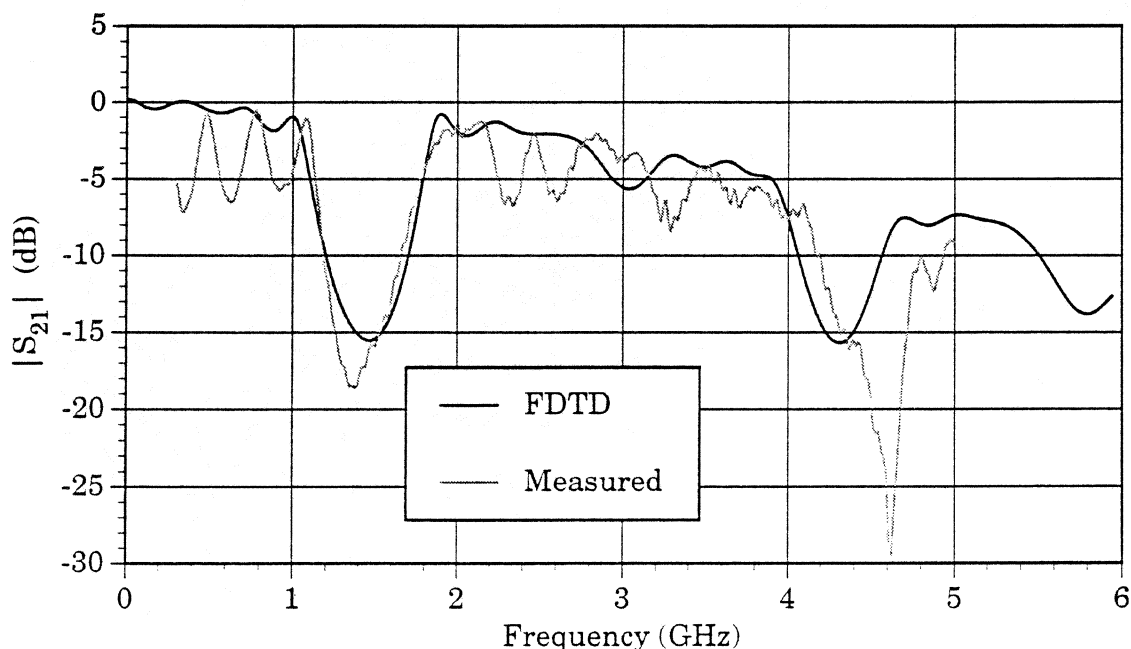


Figure 2.2 S_{21} response of the coplanar strip filter of Figure 2.1. Measurements were performed on a 1680× scale model. Scaled signal reject band is centered at 1.49 GHz and IF passband is from 4.7-7.2 MHz.

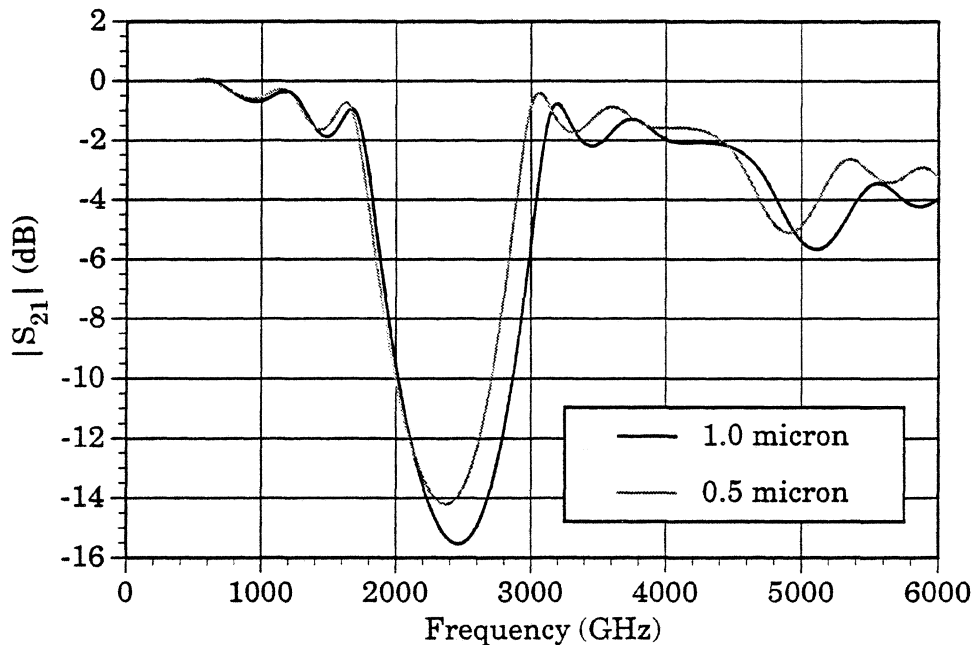


Figure 2.3 FDTD analysis of filter of Figure 2.1 with metal thicknesses of 1.0 and 0.5 μm .

that the reject bandwidth is reduced by about 10% when the metal thickness is reduced by 0.5 μm .

The coplanar strip filter was also simulated using MDS for the case where the metal thickness is 1.0 μm . In Figure 2.4, the FDTD and MDS calculations are compared. With only a small shift in the frequency response and a small difference in the magnitude, they both predict the same ripple pattern in the pass regions as well as the same cutoff frequency. The growing discrepancy in magnitude in the region beyond 4 THz is largely due to radiation loss present in the FDTD calculations but not present in the MDS simulation. This example shows that, at least for this simple filter, both the FDTD method and MDS can be used to provide useful design information about the coplanar strip filter; however, the FDTD method is able to provide more quantitatively accurate results.

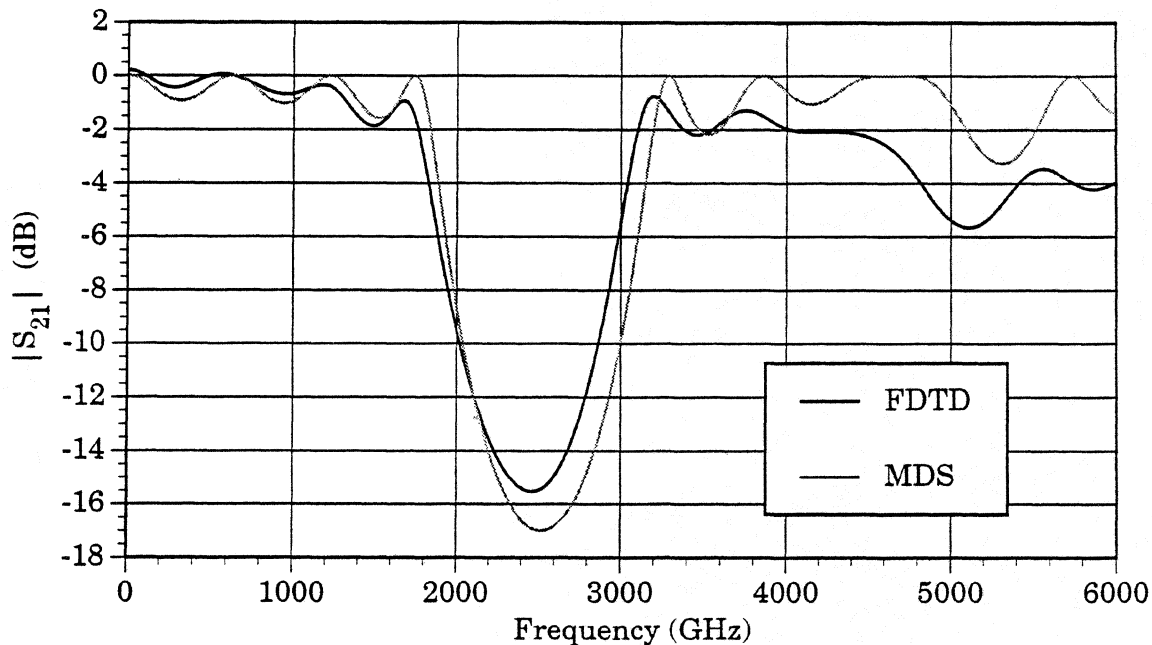


Figure 2.4 Comparison of FDTD and MDS analyses of filter of Figure 2.1

2.2 Coplanar Waveguide Filter

The good agreement obtained with the FDTD analysis and measurements on the coplanar strip filter gave us confidence to apply the FDTD method to the design of the coplanar waveguide filter shown in Figure 2.5. The function of the filter remains the same; that is, it rejects the signal band and passes the intermediate frequencies for the 2.5 THz mixer. The filter is fabricated on a GaAs ($\epsilon_r = 11.7$) substrate rather than on quartz and is meant to be used with a dual slot antenna mixer design [10] similar to that described in [11]. The final filter section lengths and widths are given in Figure 2.5. In Figure 2.6, the FDTD and MDS results are compared with fair agreement for the case of zero metal thickness. The MDS simulation does not include the radiation loss or the effect of the capacitive discontinuity between adjacent filter elements and these factors are the most likely causes of the discrepancies between the two analyses.

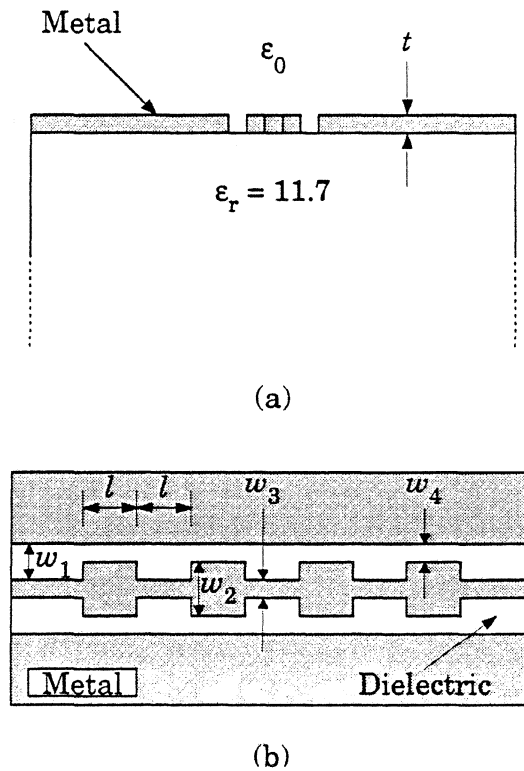


Figure 2.5 Coplanar waveguide filter (not to scale): (a) Cross section showing coplanar waveguide metal on a dielectric halfspace; (b) Top view showing metal filter pattern. Dimensions (in μm) are: $t = 0.0$, $l = 12.0$, $w_1 = 3.25$, $w_2 = 6.0$, $w_3 = 0.5$, $w_4 = 0.5$.

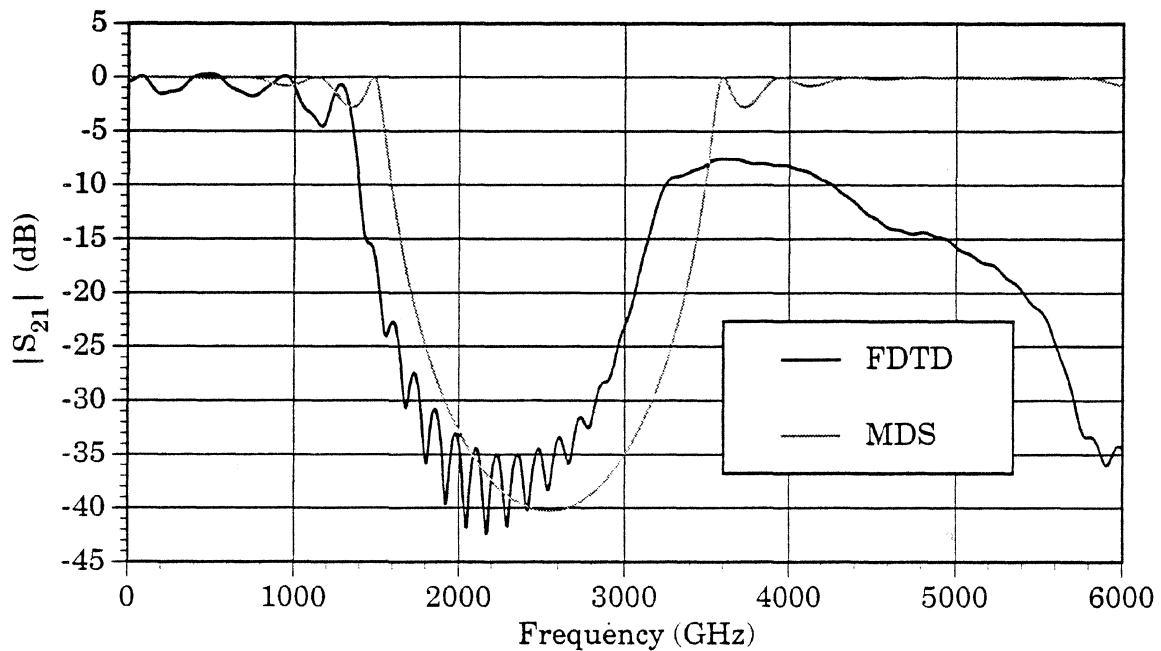


Figure 2.6 Comparison of FDTD and MDS analyses of filter of Figure 2.5.

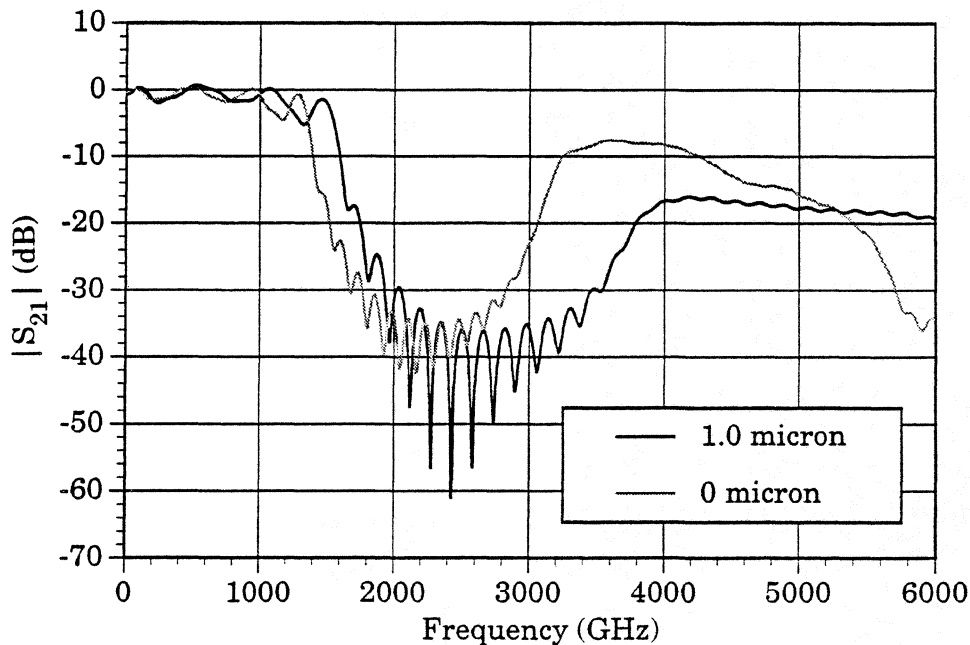


Figure 2.7 FDTD analysis of filter of Figure 2.5 with metal thicknesses of 1.0 and 0.0 μm .

The coplanar waveguide filter is also considered for the case where the metal thickness is 1.0 μm . In Figure 2.7, the FDTD calculations for the same filter with different metal thickness are compared. The effect of increasing the metal thickness is to shift the cutoff up in frequency by 10% as well as to increase the width of the stop band by about 20%.

3 Post-Gap Mounting Structure

Typical millimeter wave mixer (or multiplier) mounting structures combine waveguide and microstrip circuits for coupling energy into and out of a nonlinear device. The design and characterization of these structures is complicated by the often complex geometries and by the multimodal nature of the structure. Often, low frequency scale model measurements are employed to derive the impedances which the mount can present to the nonlinear element (such as a Schottky diode) over the

frequency range of interest. These impedances must be known at the LO and RF frequencies as well as at all relevant higher harmonic sidebands. Analytical methods [1, 12, 13] can be used to calculate the driving point impedance and derive equivalent circuits for simple waveguide mounts; however, the accuracy of the results is limited by the simplifying assumptions underlying the methods.

The FDTD method is an ideal technique for analyzing such structures. A single simulation can provide impedance information over the entire frequency range of interest, and the flexibility of this method allows for easy modeling of a wide range of mount designs. As a first step in applying the FDTD analysis to a complex waveguide mount, the simple mount of Figure 3.1, composed of a set of shorted square posts protruding towards the center of the E-plane wall of a full height rectangular waveguide, is analyzed. One end of the waveguide is terminated with a backshort

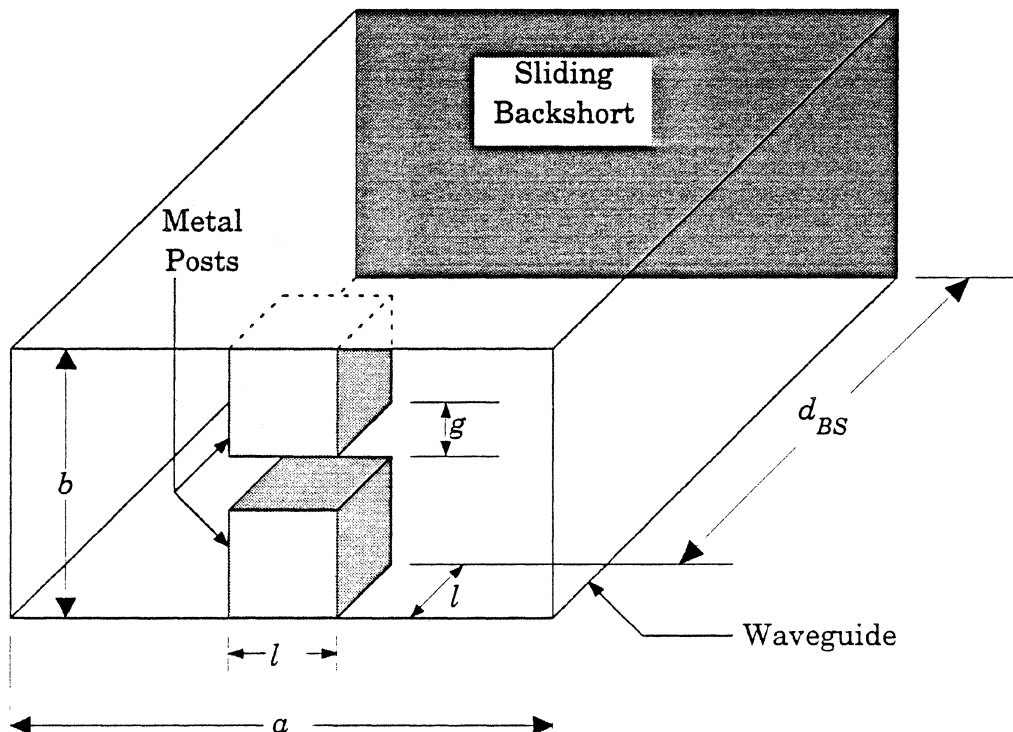


Figure 3.1 Post-gap waveguide mounting structure. Dimensions (in cm) for the 8 GHz scale model are: $a = 2.54$, $b = 1.27$, $l = 0.762$, $g = 0.381$; d_{BS} has settings of 0.4, 0.8, 1.2, 1.6, 2.0 and 2.4 cm.

tuning element while the other end is considered to be matched to free space. The impedance is calculated at the centered gap in the posts where a non-linear device might be located. The analysis is supported by experimental measurements on an 8 GHz mount model. In addition to the measurements and FDTD modeling, the mount is also characterized by the method developed by Eisenhart and Khan [1].

3.1 Measurement Technique

The embedding impedance of the post-gap mount of Figure 3.1 is measured on an 8 GHz scale model using the buried coaxial probe technique of Eisenhart and Khan [1]. A small UT85 (0.085" outer diameter) coaxial cable extends through a small hole in one of the protruding posts with the outer conductor and dielectric cut so they are flush with the face of the post. The inner conductor of the coax extends across the gap and is electrically connected to the second post. The opposite end of the cable is then connected to an HP8510 network analyzer for measurement. During the calibration of the HP8510, the reference plane is moved to the face of the first post. On one side of the post-gap mount, the waveguide is terminated with a contacting sliding backshort. On the other side the waveguide is terminated with a tapered absorber to simulate a matched condition. Measurements are taken in the frequency range 8-13 GHz for six different backshort settings: $d_{BS} = 0.4, 0.8, 1.2, 1.6, 2.0$ and 2.4 cm where d_{BS} is as shown in Figure 3.1.

3.2 FDTD Analysis

The structure is numerically modeled using space step sizes $\Delta x = \Delta z = 0.9525$ mm and $\Delta y = 0.5080$ mm. The waveguide cross section is $26\Delta x \times 25\Delta y$, while the posts are $8\Delta x \times 8\Delta z$ and centered in the x direction of the waveguide. The six backshort settings of 0.4, 0.8, 1.2, 1.6, 2.0 and 2.4 cm are modeled, respectively, as $4\Delta z, 8\Delta z, 13\Delta z, 17\Delta z, 21\Delta z$ and $26\Delta z$. The gap size of $g = 0.254$ cm is modeled as $5\Delta y$.

The waveguide walls and the backshort are modeled as perfect conductors so the electric fields tangential to these surfaces are forced to be zero. The remaining boundary, representing the open ended waveguide, is located far from the posts so that no reflections from this boundary can reach the points of interest during the computation, thus simulating a matched waveguide condition. This step was necessary to avoid the small amount of reflections caused by first order absorbing boundaries which can adversely affect the frequency domain results.

Fields are excited between the centers of the faces of the two posts by using a matched source condition [14]. Since the post faces are separated by five nodes, a source conductance of $\sigma = 56.0 (\Omega\text{m})^{-1}$ is chosen to simulate a 50Ω source. The fields are excited as Gaussian pulses in time with $T = 1/2f_{\text{max}} = 35.71$ ps chosen to cover up to 14 GHz. The time step is chosen to be $\Delta t = 1.02$ ps and the simulation is performed for 4300 time steps. At each time step the voltage and current between the two posts is calculated and after the simulation the impedance is found by taking the ratio of the Fourier transform of the voltage to the Fourier transform of the current.

The input impedance of the post-gap mount is calculated as a function of frequency in the range 8-13 GHz for each of the six backshort positions. Figures 3.2a and 3.2b compare the computed and measured real and imaginary parts of the input impedance for backshort settings of 1.6 and 2.4 cm, respectively. In Figure 3.3, the measured and computed input impedance as a function of backshort position at $f = 8.5$ GHz are compared.

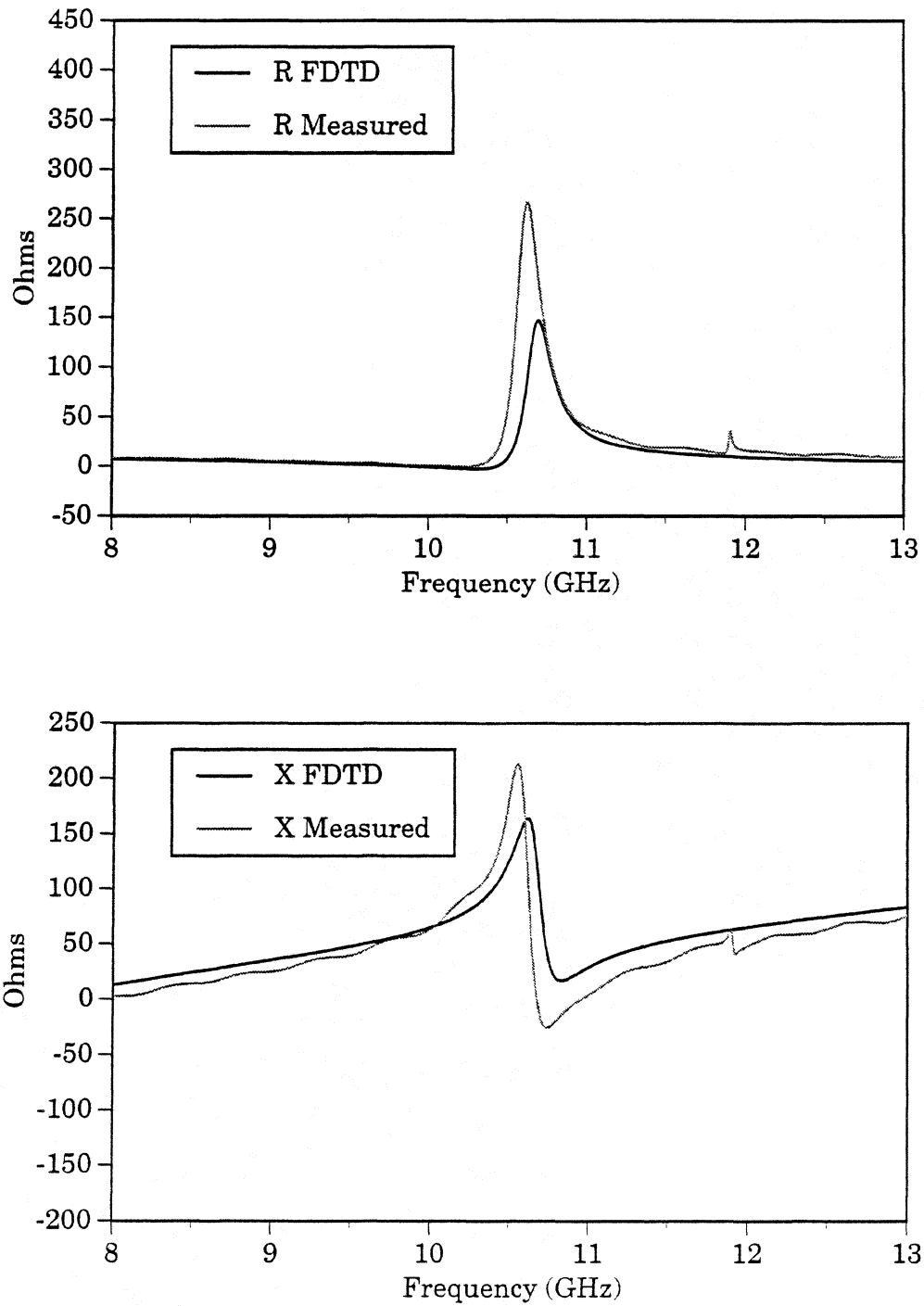


Figure 3.2a FDTD and measured real (R) and imaginary (X) parts of the input impedance for the mount of Figure 3.1 with $d_{BS} = 1.6$ cm.

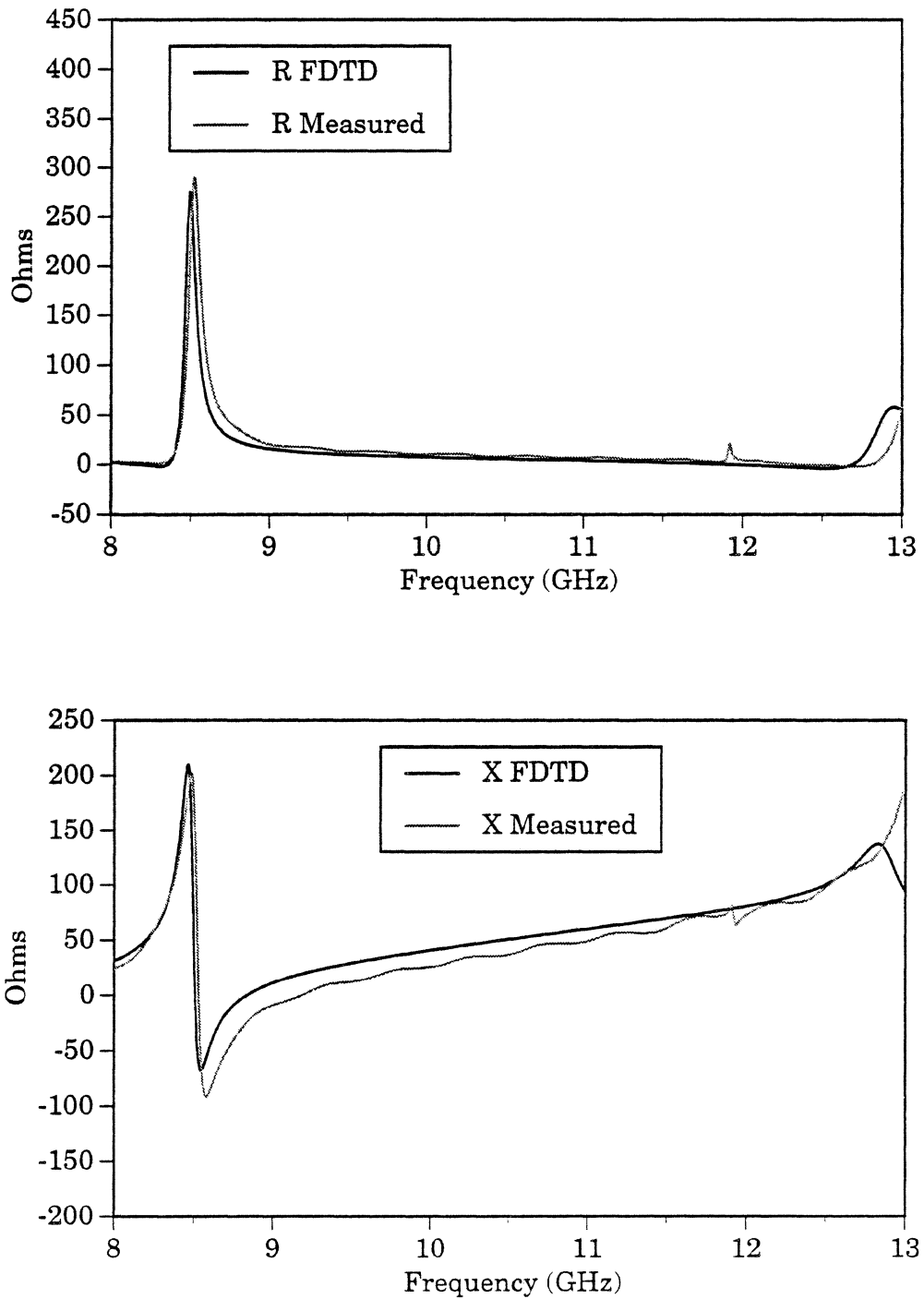


Figure 3.2b FDTD and measured real (R) and imaginary (X) parts of the input impedance for the mount of Figure 3.1 with $d_{BS} = 2.4$ cm.

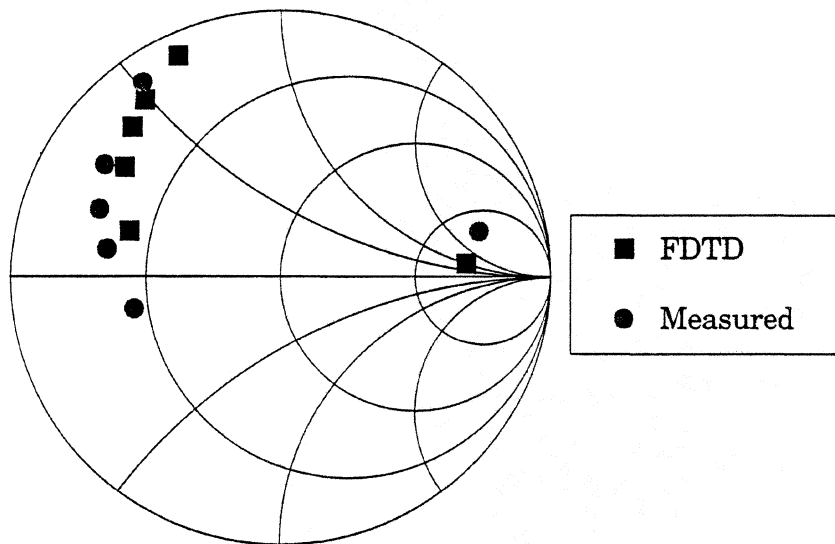


Figure 3.3 FDTD and measured post-gap mount input impedance as a function of backshort setting at $f = 8.5$ GHz.

Figures 3.2 and 3.3 show good agreement between the computed and measured input impedances for this mount. The slight difference between the measured and computational values of the impedance at resonance is attributed to an uncertainty in the exact position of the shorting plane of the sliding backshort in the model. The phase difference in Figure 3.3 is attributed to the effects of fringing capacitance at the end of the probe cable, which is not present in the calculations, and to the fact that the experimental and computational reference planes are slightly different.

3.3 Theoretical Analysis

A theoretical expression for the embedding impedance of a post-gap mounting structure has been derived by Eisenhart and Khan [1]. The analysis is strictly valid only for flat strips. As such, the three-dimensional posts are approximated by equivalent flat strips of zero thickness. Also, this method imposes restrictions on the normalized gap size ($g' = g/b < 0.25$, where g is the gap size and b is the waveguide height) and the normalized strip width ($w' = w/a < 0.25$, where w is the strip width and a is the waveguide width). The derivation of the impedance expression involves the

dyadic Green's function for a waveguide and the expansion of the electric field and current density into sets of orthogonal functions.

In testing their theoretical expression for the mount impedance, Eisenhart and Khan considered posts which are circular with a diameter, d . These posts are subsequently replaced by equivalent flat strips of effective width, $w = 1.8d$. In this same vein the square posts of the mount in Figure 3.1 are substituted with circular posts of the same cross sectional area, or of diameter, $d = 2l/\sqrt{\pi}$. Then, the strip width is approximated as $w = 1.8d = 1.548$ cm.

This Eisenhart and Khan analysis is applied to the post-gap mount for each of the six backshort settings over the frequency range 8-13 GHz. In Figures 3.4a and 3.4b the theoretical and measured mount impedances are compared as a function of frequency for the backshort settings of $d_{BS} = 1.6$ and 2.4 cm, respectively. Figure 3.5 compares the theoretical input impedance with the FDTD calculations and the measurements as a function of backshort position at $f = 8.5$ GHz.

Figures 3.4 and 3.5 indicate a considerable amount of error in the theoretical impedance. However, this is not unexpected as the posts are rather large and, in fact, the normalized strip width used to approximate the posts is larger than what is allowed by the analysis ($w' = w/a = 0.61 > 0.25$). Nevertheless, this method still does a decent job of predicting the resonant frequency of the structure if the uncertainty of the experimental backshort setting is taken into account. However, this example points out that although the FDTD method requires more computer time and memory to run, it does an excellent job of properly calculating the impedances and at the same time offers much greater flexibility in the structures which can be analyzed.

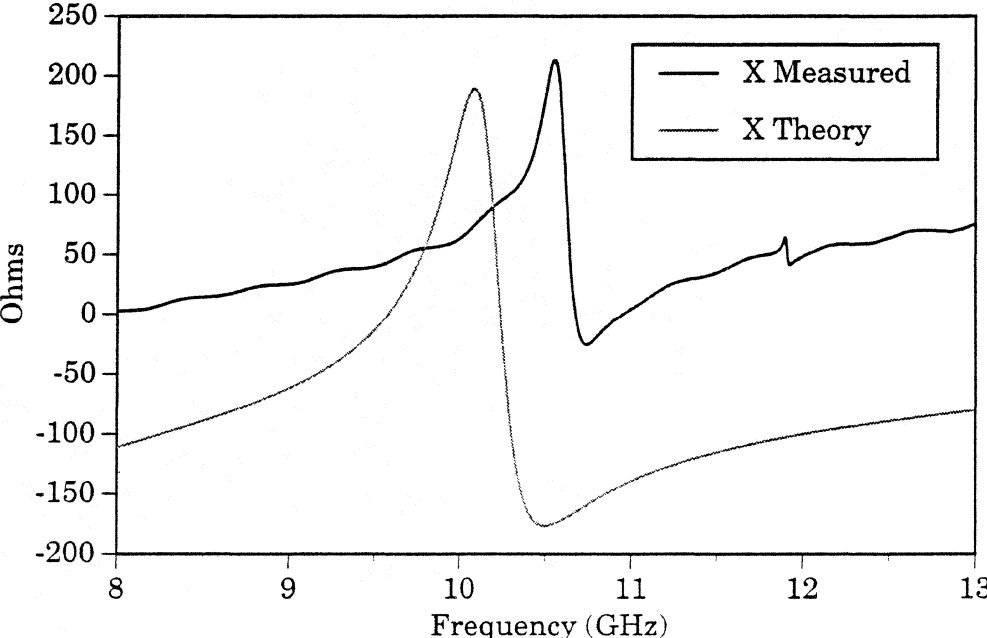
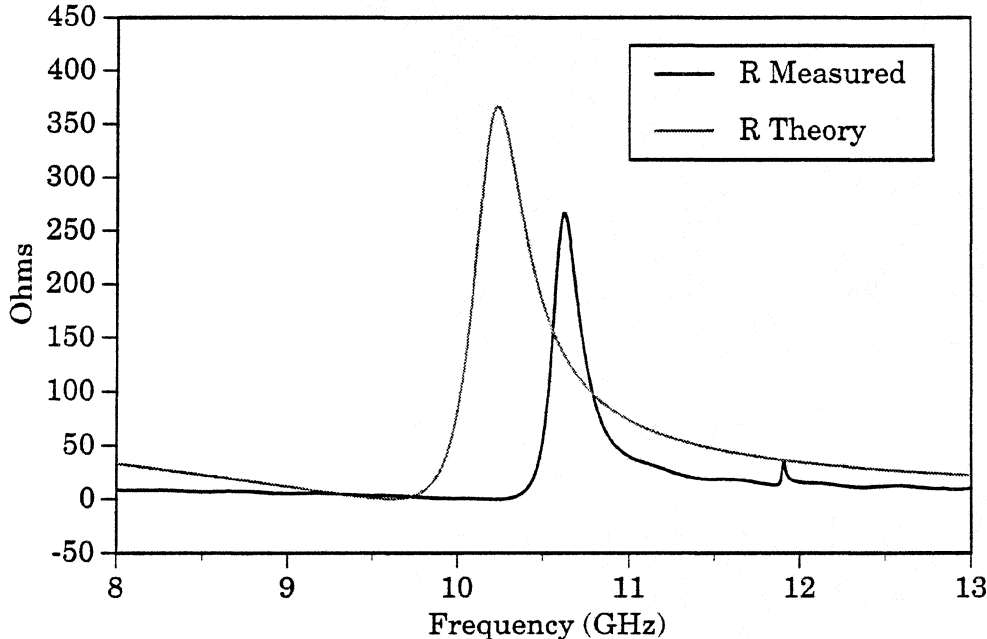


Figure 3.4a Theoretical [1] and measured real (R) and imaginary (X) parts of the input impedance for the mount of Figure 3.1 with $d_{BS} = 1.6$ cm.

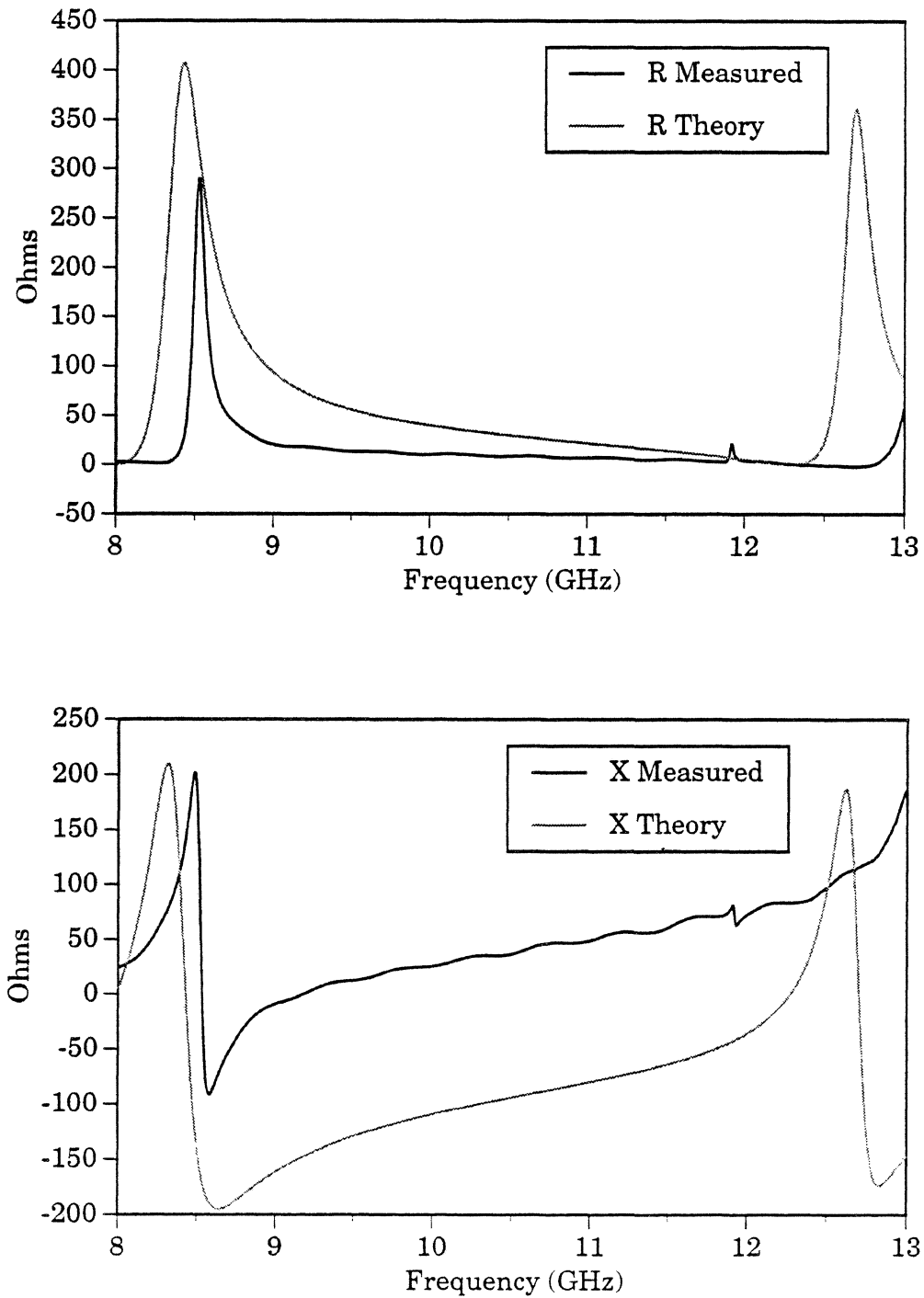


Figure 3.4b Theoretical [1] and measured real (R) and imaginary (X) parts of the input impedance for the mount of Figure 3.1 with $d_{BS} = 2.4$ cm.

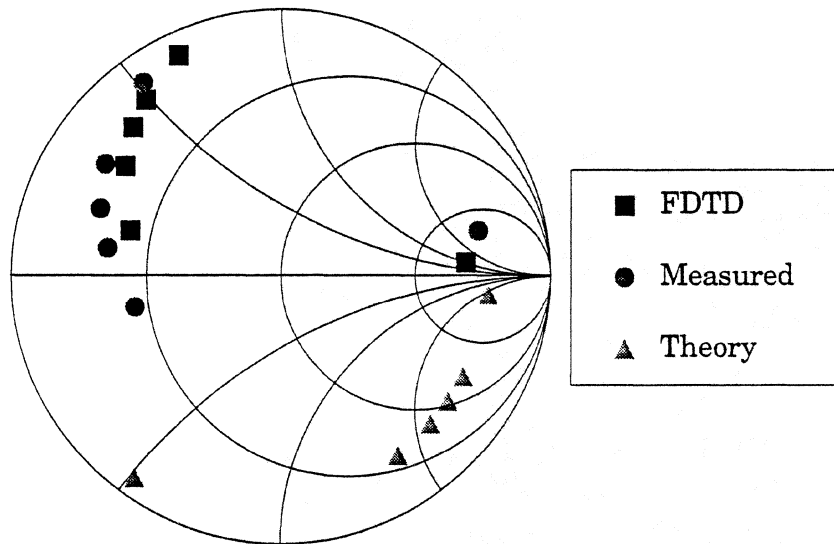


Figure 3.5 FDTD, measured and theoretical [1] post-gap mount input impedance as a function of backshort setting at $f = 8.5$ GHz.

4 Conclusions

We have demonstrated the utility of the FDTD method for problems in the millimeter and submillimeter wave bands. Good agreement between the FDTD calculations and scale model measurements and/or MDS simulations has been achieved in the analysis of the coplanar filter structures and the simple post-gap waveguide mounting structure. We are currently employing the FDTD method to analyze a coplanar waveguide fed twin-slot antenna, and preliminary results are encouraging.

Although the ability to accurately simulate the above mentioned structures is in and of itself a useful and important capability, more often these structures are only a part of a larger system whose characterization is desired. For example, the coplanar waveguide filter studied in this paper must be carefully designed to perform the proper signal separation; however, it must also interface properly with the antenna and active device structure it is meant to feed. The memory and speed available in modern computing environments allow us to begin to consider extending the FDTD

method to the analysis of much larger problems. An example which would be of interest to many researchers working with millimeter-wave mixers and frequency multipliers would combine waveguide tuning and coupling circuits with microstrip filter circuits to analyze the complete mounting structure. In addition, some researchers are also considering active device characterization [15, 16] as part of the FDTD analysis which would allow not only passive mount parameters to be determined, but also the complete nonlinear system to be characterized. Over the next several years, the FDTD method will continue to increase in importance as a unique tool for the characterization of millimeter and submillimeter wave structures.

Bibliography

- [1] R. L. Eisenhart and P. J. Khan, "Theoretical and Experimental Analysis of a Waveguide Mounting Structure," *IEEE Trans. Microwave Theory Tech.*, Vol. MTT-19, No. 8, pp. 706-719, August 1971.
- [2] K. S. Yee, "Numerical Solution of Initial Boundary Value Problems Involving Maxwell's Equations in Isotropic Media," *IEEE Trans. Antennas Prop.*, Vol. AP-14, No. 3, pp. 302-307, May 1966.
- [3] P. H. Siegel, J. E. Oswald, R. J. Dengler, D. M. Sheen and S. M. Ali, "Measured and Computed Performance of a Microstrip Filter Composed of Semi-insulating GaAs on Fused Quartz Substrate," *IEEE Microwave and Guided Wave Letters*, Vol. 1, No. 4, pp. 78-80, April 1991.
- [4] A. Reineix and B. Jecko, "Analysis of Microstrip Patch Antennas Using Finite Difference Time Domain Method," *IEEE Trans. Antennas Prop.*, Vol. 37, No. 11, pp. 1361-1369, November 1989.
- [5] D. M. Sheen, S. M. Ali, M. D. Abouzahra and J. A. Kong, "Application of the Three-Dimensional Finite-Difference Time-Domain Method to the Analysis of Planar Microstrip Circuits," *IEEE Trans. Microwave Theory Tech.*, Vol. 38, No. 7, pp. 849-857, July 1990.
- [6] P. Alinikula and K. S. Kunz, "Analysis of Waveguide Aperture Coupling Using the Finite-Difference Time-Domain Method," *IEEE Microwave and Guided Wave Letters*, Vol. 1, No. 8, pp. 189-191, August 1991.

- [7] N. I. Dib and L. P. B. Katehi, "Analysis of the Transition from Rectangular Waveguide to Shielded Dielectric Image Guide Using the Finite-Difference Time-Domain Method," *IEEE Microwave and Guided Wave Letters*, Vol. 3, No. 9, pp. 327-329, September 1993.
- [8] Z. Bi, Y. Shen, K. Wu and J. Litva, "Fast Finite-Difference Time-Domain Analysis of Resonators Using Digital Filtering and Spectrum Estimation Techniques," *IEEE Trans. Microwave Theory Tech.*, Vol. 40, No. 8, pp. 1611-1619, August 1992.
- [9] P. H. Siegel, "A Submillimeter-wave Heterodyne Array Receiver Using a Dielectric-filled Parabola: Concept and Design," First International Symposium on Space Terahertz Technology, Ann Arbor, Michigan, pp. 218-234, March 1990.
- [10] P. H. Siegel, "An Open-Structure Mixer Using an All-GaAs Integrated Diode/Antenna Wafer for Millimeter and Submillimeter Wavelengths," Jet Propulsion Laboratory New Technology report #8972, 7 pgs., January 1994.
- [11] G. Gauthier, T. P. Budka, W. Y. Ali-Ahmad, D. F. Filipovic and G. M. Rebeiz, "A Low Noise 86-90 GHz Uniplanar Schottky-Receiver," IEEE International Symposium on Microwave Theory and Techniques, Atlanta, GA, pp. 325-328, June 1993.
- [12] R. L. Eisenhart, "Discussion of a 2-Gap Waveguide Mount," *IEEE Trans. Microwave Theory Tech.*, Vol. MTT-24, No. 12, pp. 987-990, December 1976.
- [13] J. S. Joshi and J. A. F. Cornick, "Analysis of Waveguide Post Configurations," *IEEE Trans. Microwave Theory Tech.*, Vol. MTT-25, No. 3, pp. 169-181, March 1977.
- [14] D. M. Sheen, "Numerical Modeling of Microstrip Circuits and Antennas," Ph.D. Dissertation, Department of Electrical Engineering and Computer Science, Massachusetts Institute of Technology, Cambridge, MA, June 1991.
- [15] W. Sui, D. A. Christensen and C. H. Durney, "Extending the Two-Dimensional FDTD Method to Hybrid Electromagnetic Systems with Active and Passive Lumped Elements," *IEEE Trans. Microwave Theory Tech.*, Vol. 40, No. 4, pp. 724-730, April 1992.
- [16] B. Toland, B. Houshmand and T. Itoh, "Modeling of Active Regions with the FDTD Method," *IEEE Microwave and Guided Wave Letters*, Vol. 3, No. 9, pp. 333-335, September 1993.